King Saud University

Arabian Journal of Chemistry

www.ksu.edu.sa
www.sciencedirect.com

ORIGINAL ARTICLE

Improved simultaneous adsorption of Cu(II) and Cr(VI) of organic modified metakaolin-based geopolymer

Zefeng Yu, Weifeng Song *, Jiayao Li, Qiuhua Li

School of Environmental Science and Engineering, Guangdong University of Technology, Guangzhou 510006, PR China

Abstract   In this paper, a metakaolin-based mesoporous geopolymer (GP-CTAB) was used as adsorbent for Cu(II) and Cr(VI) through a novel and simple synthetic route using cetyltrimethylammonium bromide (CTAB) as an organic modifier. The application of GP-CTAB for the simultaneous removal of metal anions and cations in aqueous solution was studied for the first time. The results of X-ray diffraction (XRD) spectroscopy, Fourier transform infrared (FTIR) spectroscopy, Brunauer, Emmett and Teller (BET), and Barrett, Joyner, and Halenda (BJH) methods indicate that GP-CTAB is still geopolymer even in the presence of quaternary ammonium salt cations. The material was tested to simultaneously adsorb Cu(II) and Cr(VI) from an aqueous solution. The results show that GP-CTAB can adsorb anions simultaneously without sacrificing the adsorption properties of heavy metal cations, which is superior to conventional geopolymers. The maximum theoretical adsorption capacity of GP-CTAB for Cu(II) and Cr(VI) was 108.2 mg/g and 95.3 mg/g in the binary system, respectively. It was also found that the presence of Cu(II) in the solution promoted the adsorption of Cr(VI). Given this characteristic of GP-CTAB, it has shown great application prospects in the prevention and control of heavy metal pollution.

1. Introduction

Geopolymer (GP), also known as a soil polymer or inorganic polymer, was first proposed by Davidovits et al. (1994). GP is a

* Corresponding author.
  E-mail address: weifengsong@gdut.edu.cn (W. Song).
Peer review under responsibility of King Saud University.

Production and hosting by Elsevier

three-dimensional network of inorganic polymers prepared by acid or alkaline activation of aluminosilicate-containing metakaolin or solid waste such as fly ash (Ding et al., 2019; Morsy et al., 2014; Louati et al., 2016; Provis 2014). Although most of the research on GPs has focused on the application of concrete building materials, it has been considered for wastewater treatment applications (Qiu et al., 2018; Javadian et al., 2015; Messina et al., 2017). Due to the remarkable properties of GPs in aqueous solution, and its low cost and lack of secondary pollution, GP metal adsorption performance has attracted more and more attention (Lee et al., 2017; Siyal et al., 2018). Na$^+$ or K$^+$ wrapped by the GP tetrahedral struc-

ture can be ion-exchanged with external cations and has a rich medium porosity (Naghsh and Shams 2017). Therefore, some work focuses on the application of this material to remove pollutants such as metals ions (essentially cationic) and dyes (Li et al., 2006; Kara et al., 2017; Barbosa et al., 2018; Naghsh and Shams 2017).

Although GP has been studied in the field of heavy metal adsorption, rare studies have been done to effectively adsorb heavy metals in the form of anions like Cr(VI) (Lee et al., 2017; Liu et al., 2016; Maleki et al., 2019). Organic modification of kaolin with surfactants, then electrostatic adsorption via organic functional groups on the surface is a approach for heavy metal anions removal from wastewater. The disadvantage of this idea, however, is that the adsorption performance of cations is not ideal (Lee and Kim 2002; Li et al., 2006; Li et al., 2007). In the wastewater produced by surface treatment industries such as electroplating, there is often more than one heavy metal, and cations and anions are also present in large quantities. These ions are toxic, bioaccumulate, non-biodegradability, and flow in natural water ecosystems, so they are categorised as major pollutants (Landaburu-Aguirre et al., 2010; Wan Ngah and Hanafiah 2008). Neither GP nor the organically modified kaolin can simultaneously adsorb the anion and cation and achieve satisfactory adsorption.

Some research uses cetyltrimethylammonium bromide (CTAB), sodium lauryl sulfate (K12), and other surfactants in the preparation of GP (Singhal et al., 2017; Tang et al., 2018), but only as a blowing agent to increase the GP-specific surface area during curing, not for other modifying uses. Also, in the adsorption performance test of pollutants, most of the studies only carried out adsorption in a single system, and only a few studied the co-adsorption behaviour of binary systems, especially cations and anions. In particular, it has been reported that the longer the carbon chain length of the surfactant, the better the adsorption performance of the adsorbent. Therefore, the cationic surfactant CTAB having a longer carbon chain was selected (Liang et al., 2016; Cai et al., 2019). This study intends to simultaneously perform alkaline activation and organic modification of metakaolin by adding quantitative amounts of CTAB during the fabrication of GP. The quaternary ammonium salt cation is carried on the surface without changing the tetrahedral structure of the GP to obtain the effect of simultaneously adsorbing heavy metals in the form of anions and cations.

2. Materials and methods

2.1. Materials and chemicals

The metakaolin used for this study was obtained via kaolin dehydration at 800 °C in a muffle furnace for 2 h. Its major chemical components are listed in Table 1. Kaolin, NaOH, NaAlO$_2$, Na$_2$SiO$_3$·5H$_2$O, CuSO$_4$·5H$_2$O, and CTAB used were supplied by Aladdin Ltda. (Shanghai, China). K$_2$Cr$_2$O$_7$ was

purchased from Guangzhou Chemical Reagent Factory (Guangzhou, China). All of the above are solid reagents. All solutions were prepared using deionised water.

2.2. Synthesis and characterisation

NaOH, NaAlO$_2$, Na$_2$SiO$_3$·5H$_2$O were used to prepare an alkaline activator solution at a molar ratio of 1: 1.3: 2.8. Then metakaolin was added: alkaline activator: CTAB = 1.5 g: 50 mL: 0.5 g, which formed geopolymer precursor. This precursor was then cast into a reactor for 24 h at 30 °C and 180 revs/min. Upon finishing the reaction, the solid particles were filtered and washed with distilled water until neutral. The resulting product was stirred with water, the precipitate was allowed to stand, and the liquid was discarded to leave a precipitate. The procedure was repeated until the pH of the supernatant was neutral. The precipitate was added with a little water and centrifuged at 6000 revs/min for 5 min. The precipitate was collected, dried in an oven at 65 °C, and then ground and sieved (≥110 mesh). A flow-chart of the preparation process is shown in Fig. 1. GP sample for comparison was
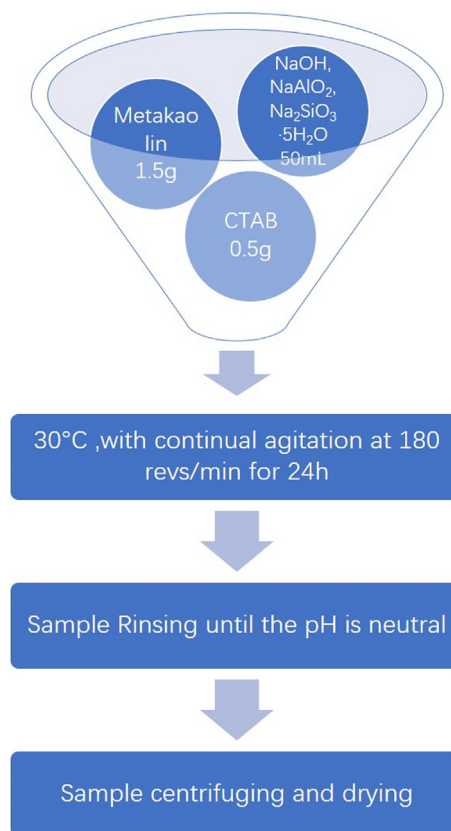

Fig. 1 Flow-chart of the preparation of geopolymer-cetyltrimethylammonium bromide (GP-CTAB).

Table 1 Chemical composition of metakaolin used in this study.

Component	SiO$_2$	Al$_2$O$_3$	TiO$_2$	Fe$_2$O$_3$	CaO	ZrO$_2$	Loss amount
Content (wt%)	48.45%	47.09%	0.70%	0.53%	0.45%	0.11%	2.67%

prepared using the same synthetic method but without adding CTAB during the preparation. The two geopolymers were named GP-CTAB and GP respectively.

The sample structure was characterised via X-ray diffraction spectroscopy (XRD; Brook, D8-XRD-7000), operated with Cu–Kα radiation (λ = 1.5418 Å), 40 kV, 2θ scan interval of 10-70° (step size was 0.5°/min). Samples were characterised via Fourier transform infrared spectroscopy (FTIR) (Thermo Fisher, Nicolet 380) in the range of 4000–500 cm^{-1} to identify the functional groups. The surface morphology of the GP was observed via scanning electron microscopy (SEM; Hitachi, SU8220). The specific surface area and micropore structure were analysed via an automatic surface and aperture analyser (Micromeritics, ASAP2020). The specific surface area, pore-volume, and pore size distribution parameters at −195.85 °C were determined by analysis of the nitrogen adsorption/desorption isotherm. The specific surface area, pore volume and pore size distribution were determined by the Brunauer, Emmett and Teller (BET), and Barrett, Joyner, and Halenda (BJH) methods, respectively.

2.3. Adsorption experiments

Batch adsorption experiments were carried out on samples to remove Cu(II)/Cr(VI) from aqueous solutions in a simple or binary system to verify the adsorption capacity of metakaolin (MK) and geopolymers (GP and GP-CTAB). The tests were done in deionised water with a thermostated agitator employing analytical chemicals. In all experiments, the solution volume was 50 mL, the stirring rate was 180 rpm, and the stirring temperature was 30 °C.

Adsorbent (0.02 g) was added to a 50 mg/L Cu(II)/Cr(VI) solution, the pH was controlled at 5, the reaction vessel was sealed, and the mixture was placed in a thermostated agitator for different contact times (0.5–1440 min). The effect of pH was studied by adjusting the Cu(II)/Cr(VI) mixed solution pH (2–7) with dilute NaOH or HCl while keeping the adsor-

bent dose (0.4 g/L) and mixing time (4 h) constant. The effect of adsorbent dose was studied by adding 0–10 g/L of adsorbent, controlling the pH at 5 and shaking for 24 h. The experiment was repeated three times for each series. Samples were filtered with a 0.45-μm membrane filter, and atomic absorption spectroscopy (AAS) was used to analyse the filtrate and measure the amount of metal extracted from the solution. The amount of metal ion adsorbed and the removal efficiency by the GP was calculated using Equations (1) and (2):

$$Q_e = \frac{(C_0 - C_e) \times V}{m} \tag{1}$$

$$R(\%) = \frac{C_0 - C_e}{C_0} \times 100\% \tag{2}$$

where C_0 represents the initial concentration (mg/L) of the metal solution, C_e represents the solution concentration after adsorption (mg/L), Q_e represents the adsorption amount (mg/g), m represents the adsorbent mass (mg), V represents the solution volume (mL), and R represents the removal efficiency.

2.4. Kinetic and isotherms studies

Pseudo-first-order kinetics (Tang et al., 2018), pseudo-second-order kinetics (Tang et al., 2018), Elovich (Barbosa et al., 2018), Weber-Morris (intraparticle diffusion) (Tang et al., 2018) and Boyb (Majeed et al., 2013) models are commonly used to determine the mechanism of metal adsorption and the factors that control the rates, according to Equations (3), (4), (5), (6) and (7) respectively.

$$\frac{1}{Q_t} = \frac{k_1}{Q_e t} + \frac{1}{Q_e} \tag{3}$$

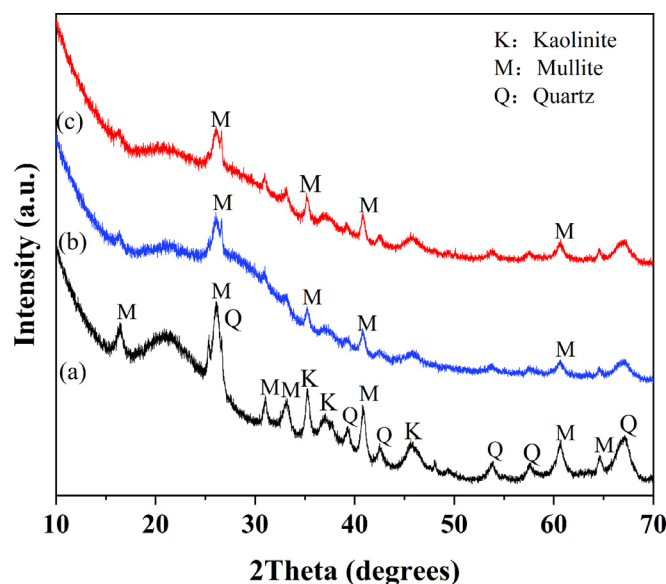$$\frac{t}{Q_t} = \frac{1}{k_2 Q_e^2} + \frac{t}{Q_e} \tag{4}$$

Fig. 2 X-ray diffraction spectra of metakaolin (MK) (a), geopolymer (GP) (b), and geopolymer-cetyltrimethylammonium bromide (GP-CTAB) (c).

$$Q_t = \frac{1}{\beta}\ln\alpha\beta + \frac{1}{\beta}\ln t \qquad (5)$$

$$Q_t = k_w t^{0.5} + C \qquad (6)$$

$$F = \frac{Q_t}{Q_\infty} = 1 - \frac{6}{\pi^2}\sum_1^\infty \left(\frac{1}{n^2}\right)\exp\left(-n^2 Bt\right) \qquad (7)$$

where Q_e (mg/g) and Q_t (mg/g) represent the number of metal ions adsorbed on the geopolymer at equilibrium and at time t (min), respectively. The constants k_1 (min^{-1}) and k_2 [g/(mg·min)] are rate constants, α is the initial adsorption rate [mg/(g·min)], and β is the rate constant (g/min) for the Elovich model. k_w is the intraparticle diffusion rate parameter [mg/(min$^{1/2}$·g)], C is the Weber-Morris model constant, Q_∞
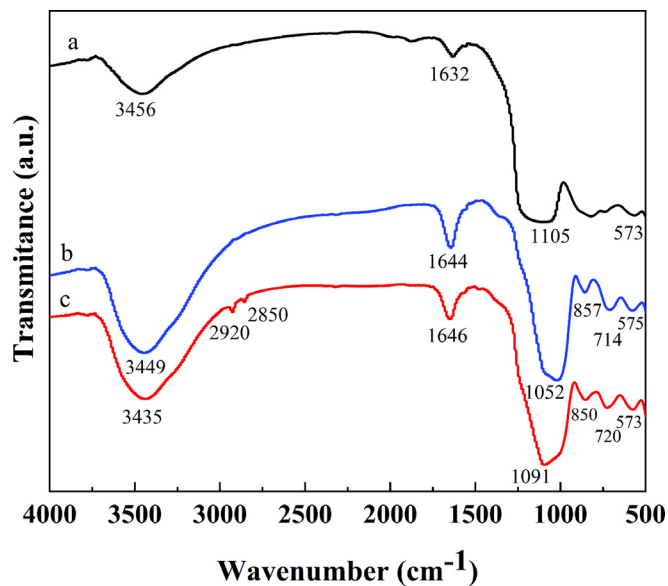

Fig. 3 The Fourier transform infrared (FTIR) spectra of the metakaolin (MK) (a), geopolymer (GP) (b), and geopolymer-cetyltrimethylammonium bromide (GP-CTAB) (c).
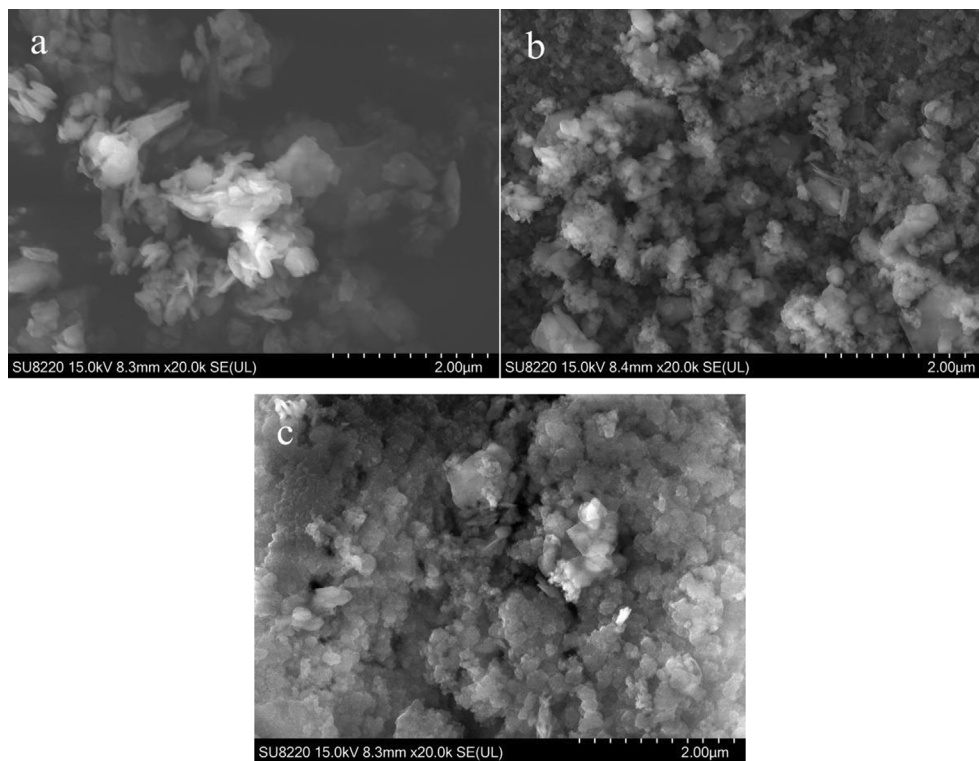

Fig. 4 Scanning electron microscopy (SEM) images of metakaolin and geopolymer (metakaolin (MK) (a), geopolymer (GP) (b), and geopolymer-cetyltrimethylammonium bromide (GP-CTAB) (c)).

(replace with Q_e) is the ultimate adsorption capacity, F is the adsorption mass fraction at time t, and drawing Bt is the ordinate, t as the abscissa of the Boyd model.

To further investigate the geopolymer adsorption behaviour of metals under varying concentrations, additional experiments were performed at a constant temperature of 30 °C to adsorb Cu(II)/Cr(VI) at different concentrations in single/binary systems. The equilibrium isotherm curves were fitted using the Langmuir (Barbosa et al., 2018), Freundlich (Barbosa et al., 2018), Temkin (Araújo et al., 2018), and Sips (Barbosa et al., 2018) models. The Langmuir isotherm (Eq. (8)) assumes monolayer adsorption onto a homogeneous surface, and its major characteristics can be expressed by the separation factor R_L (Eq. (9)). The Freundlich isotherm (Eq. (10)) assumes adsorption on a heterogeneous surface. The Temkin isotherm (Eq. (11)) assumes that the free energy of adsorption

during adsorption is the effect of its surface coverage. The Sips isotherm (Eq. (12)) is a combination of the Langmuir and Freundlich isotherm.

$$\frac{C_e}{Q_e} = \frac{1}{Q_m b} + \frac{C_e}{Q_m} \tag{8}$$

$$R_L = \frac{1}{1 + C_o b} \tag{9}$$

$$Q_e = K_f C_e^{\frac{1}{n}} \tag{10}$$

$$Q_e = \frac{RT}{b_T}\ln C_e + \frac{RT}{b_T}\ln A_T \tag{11}$$

$$Q_e = \frac{Q_{ms}(k_s C_e)^\gamma}{1 + (k_s C_e)^\gamma} \tag{12}$$

where C_e represents the equilibrium concentration of metal ions (mg/L) and Q_e represents the amount of adsorption at equilibrium (mg/g). Q_m (mg/g) and b (L/mg) are both Langmuir constants that are associated with the adsorption capacity and adsorption intensity, respectively. K_f and n are both Freundlich constants, which are related to adsorption capacity and adsorption intensity, respectively. b_T is the Temkin constant (J/mol) associated with the heat of adsorption, A_T is the Temkin isotherm equilibrium binding constant (L/mol),

Table 2 Specific surface areas and pore structures of metakaolin and geopolymers.

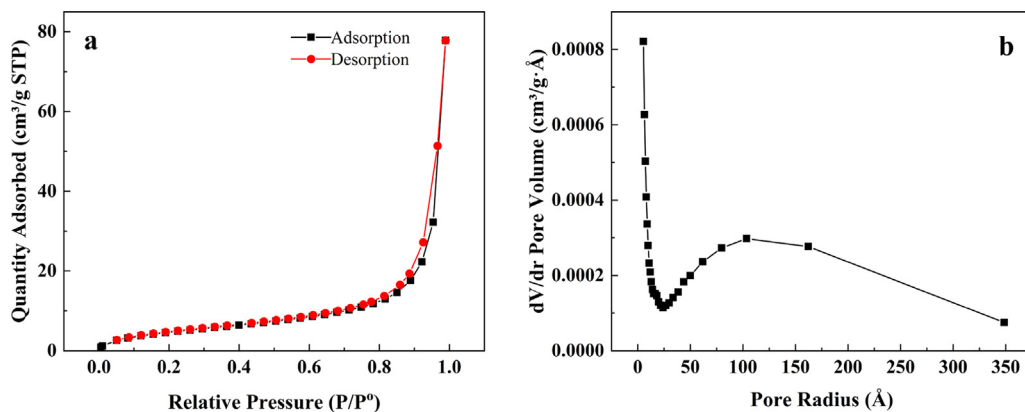|	S_{BET} (m²/g)	D_a (nm)	V_{micro} (cm³/g)
MK	3.11	1.56	0.015
GP	31.83	3.22	0.078
GP-CTAB	26.45	9.12	0.121

Fig. 5 Adsorption-desorption curve and pore size distribution of geopolymer-cetyltrimethylammonium bromide (GP-CTAB).
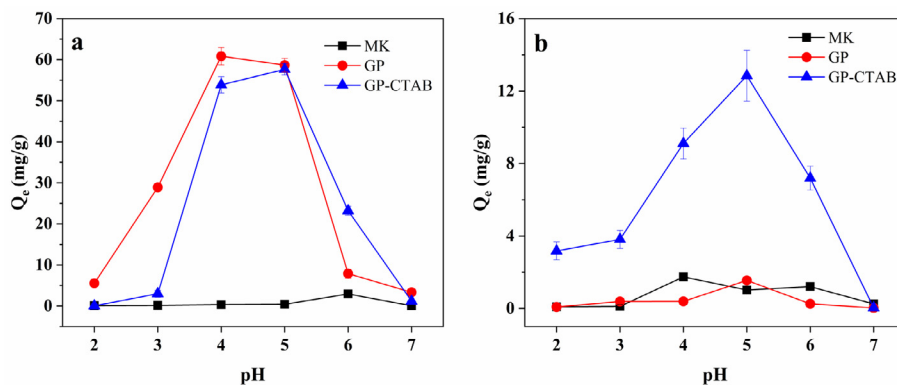

Fig. 6 Effect of pH on adsorption of (a) Cu(II) and (b) Cr(VI) (C_0 = 50 mg/L; t = 4 h; Adsorbent dose = 0.4 g/L).

R is the gas constant [8.3145 J/(mol·K)], T is the absolute temperature at 303 K, k_s is the Sips equilibrium constant, Q_{ms} is the maximum adsorption capacity (mg/g) from Sips model, and γ is the Sips exponent.

3. Results and discussion

3.1. Samples characterization

The XRD patterns for MK, GP, and GP-CTAB are shown in Fig. 2. The main crystal phase of MK is mullite, quartz, and kaolinite. After the polymerisation step, the kaolinite peak decreases as the geopolymer is produced, the XRD patterns of the GP and GP-CTAB samples show an amorphous struc-

ture with a significant reduction in most of the reflection peaks. Several peaks remain that correspond to unreacted mullite. The difference between the GP and GP-CTAB pattern is small, proving that they have the same crystalline composition.

The infrared spectra of MK, GP, and GP-CTAB are shown in Fig. 3. Broadband around 3350 cm^{-1} and a narrow band around 1640 cm^{-1} are present in all of the samples, because of the O—H stretching and the remaining adsorbed atmospheric water (Song et al., 2019; Król et al., 2016). During the polymerisation step for metakaolin, the absorption peaks at 1052 cm^{-1}, 714 cm^{-1}, and 575 cm^{-1} in the GP indicate the presence of Si—O—Si, Al—O—Si, and Si—O—Al in the octahedral structure (Mihaly-Cozmuta et al., 2014; Sarkar et al., 2017). When GP and GP-CTAB are aligned, the absorp-
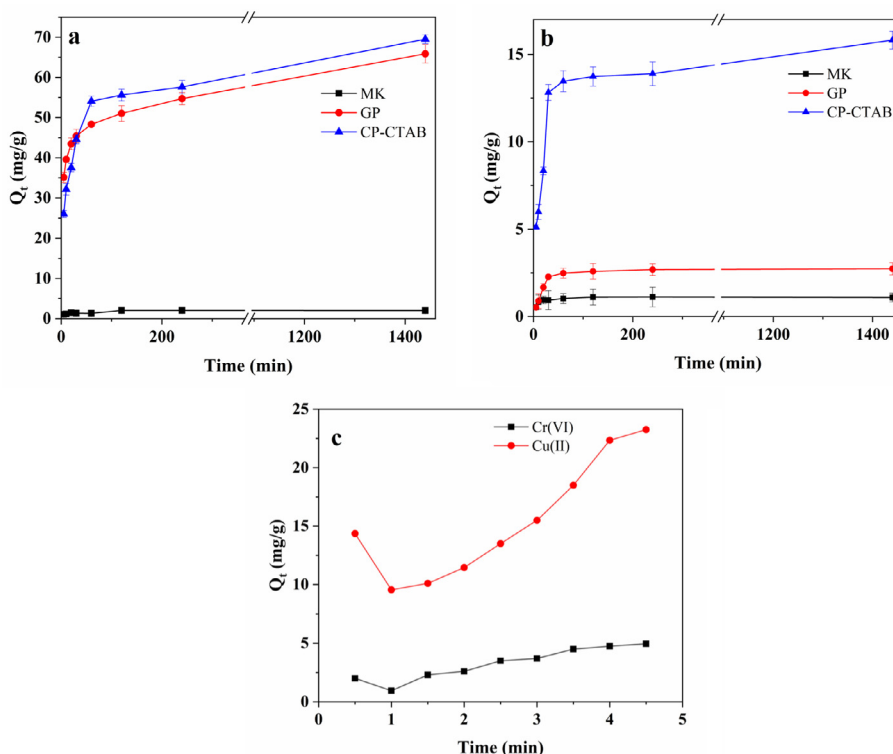

Fig. 7 Effect of contact time on adsorption of (a) Cu(II) and (b) Cr(VI), and impact of contact time by (c) geopolymer-cetyltrimethylammonium bromide (GP-CTAB) in short times (0–5 min) (C_0 = 50 mg/L; pH = 5; Adsorbent dose = 0.4 g/L).
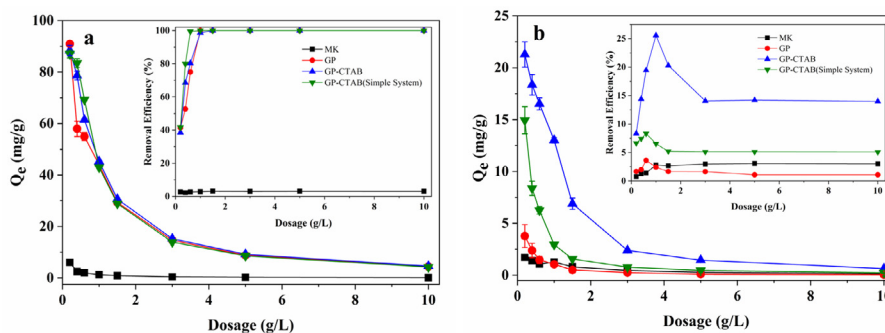

Fig. 8 Effect of adsorbent dosage on adsorption of (a) Cu(II) and (b) Cr(VI) (C_0 = 50 mg/L; pH = 5; t = 24 h).

tion peaks at 2920 cm^{-1} and 2850 cm^{-1} in GP-CTAB indicate the presence of —CH$_n$ (Xu et al., 2018; Aslan et al., 2018), confirming the presence of quaternary ammonium salt cations (CTA$^+$). At the same time, the characteristic peaks of the GP still exist in GP-CTAB, and the overall absorption peaks do not change greatly. It is proven that even if it during the organically modified, GP-CTAB only add CTA$^+$ and still belongs to the geopolymer.

SEM results are shown in Fig. 4. The metakaolin surface is irregular and loose (Fig. 4a). After the polymerisation step, geopolymer is formed with many fine particles caused by the dissolution of metakaolin into microparticles, which results from the effect of the activating agent. On the metakaolin surface, aluminium and silicon tetrahedron exist in a free form where two tetrahedra share one oxygen atom (Yunsheng et al., 2007). Then, the first rapid polymerisation of the Al-O-Si structure with an oligomeric state occurs, followed by the silicate on the surface of the slow coagulation process. The resulting structure of the geopolymer is shown in Fig. 4b and c. Compared to metakaolin, the surface of the geopolymer is regular and compact, and GP-CTAB is more compact than GP maybe because of the presence of CTA$^+$.

Table 2 presents specific surface areas (S$_{BET}$), average pore widths, and volumes of the metakaolin (MK) and geopolymers (GP and GP-CTAB). N$_2$ adsorption-desorption isotherms and pore size distribution curves of the GP-CTAB are shown in Fig. 5. According to the classification of the International Union of Pure and Applied Chemistry (IUPAC), the corresponding isotherm for the geopolymer was indicative of a type IV isotherm and a distinct H3 hysteresis loop, which is characteristic of mesoporous materials (Ding et al., 2019). The S$_{BET}$ of the geopolymer increased from 3.11 m^2/g for the metakaolin to 31.83 m^2/g (GP) and 26.45 m^2/g (GP-CTAB), since the adsorption effect greatly improved, and the S$_{BET}$ of GP-CTAB is lower than that of GP due to the attachment of CTA$^+$ (Cai et al., 2019). The pore volume and pore size of the geopolymer increased, but the values of GP-CTAB were more significant than those of GP. Among GP-CTAB samples, the largest pore size was 9.12 nm and belonged to mesopores (2–50 nm) which are favourable for adsorption.

The results in this section demonstrate the synthesis of geopolymers and show that the addition of CTAB to the synthesis step improves the properties of the geopolymer. The use of CTAB provided material with higher pore volume and diameter, and also still belongs to the geopolymer containing functional groups (CTA$^+$). These characteristics have a certain promotion effect on the adsorption of Cu(II) and Cr(VI).

3.2. Effect of pH

The effect of the initial solution pH is shown in Fig. 6. Under alkaline conditions, Cu(II) produces hydroxide precipitates, and during the pH adjustment process using NaOH, some Cu(II) is inevitably converted to precipitate. Therefore, the ini-
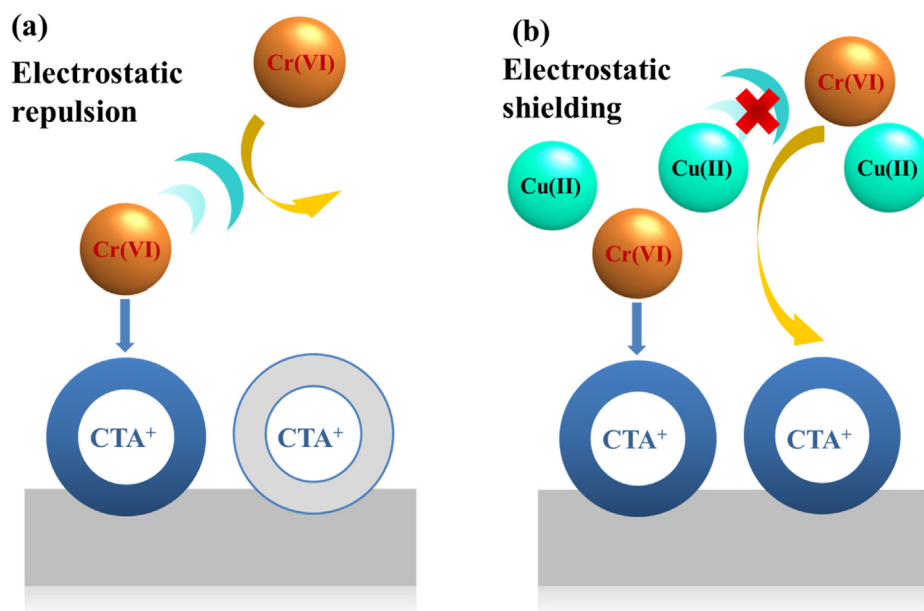
Fig. 9 Schematic diagram of the shielding effect of Cu(II) on the electrostatic repulsion between Cr(VI) (a) without Cu(II), (b) with Cu (II). When the colour of the CTA$^+$ group changes from grey to blue, the adsorption site becomes available.

Table 3 Effect of adding geopolymer-cetyltrimethylammonium bromide (GP-CTAB) on the pH of the solution.

Sorbent dose (g/L)	Cu(II)/Cr(VI) binary system (50 mg/L each)							Deionized water
	0.2	0.4	0.6	1.0	1.5	3	5	1.0
PH before adsorption					5.01			
PH after 24 h	5.15	5.36	5.50	6.16	6.72	7.62	7.93	5.07

tial concentration of Cu(II) is less than 50 mg/L under partial pH conditions. When the pH is greater than 7, there is no Cu(II) present in the initial solution. The pH range chosen is 2–7 to avoid the influence of precipitation on the adsorption effect (Mihaly-Cozmuta et al., 2014). As shown in Fig. 6, the adsorption tendency of two geopolymers for two metal ions is about the same. In general, the adsorption capacity of Cu(II) order is GP > GP-CTAB > MK, and Cr(VI) is GP-CTAB > GP > MK.

At low pH, the H^+ ions and Cu(II) in the solution compete with each other, which hinders the adsorption process of Cu(II). The adsorption effect of both geopolymers on Cu(II) is inferior. As the pH increases, the competition becomes weaker because the H^+ ion concentration decreases. The adsorption capacity of Cu(II) by both geopolymers gradually increases and is the highest in the pH range of 4–5, and the

difference is not significant. At pH > 5, the initial concentration of Cu(II) in the solution is lowered due to the pH adjustment, so that the adsorption capacity is gradually reduced. GP has a very low adsorption capacity for Cr(VI) in this pH range. When the solution is strongly acidic (pH < 3), Cr(VI) exists in the form of electrically neutral H_2CrO_4, which is not conducive to adsorption, so the adsorption capacity of GP-CTAB is low. When pH < 5, Cr(VI) is mainly in the form of $HCrO_4^-$ and a small quantity of $Cr_2O_7^{2-}$. $HCrO_4^-$ is a negative monovalent ion. When interacting with adsorbents, $HCrO_4^-$ required the least adsorption free energy and occupied the fewest active sites (Xu et al., 2019; Cai et al., 2019). When pH > 5, $HCrO_4^-$ rapidly transforms into CrO_4^{2-} with increasing pH. As a negative divalent ion, CrO_4^{2-} requires more adsorption free energy and occupies more active sites than $HCrO_4^-$. At the same time, OH^- anions will release the adsorbed $HCrO_4^-$ decomposed
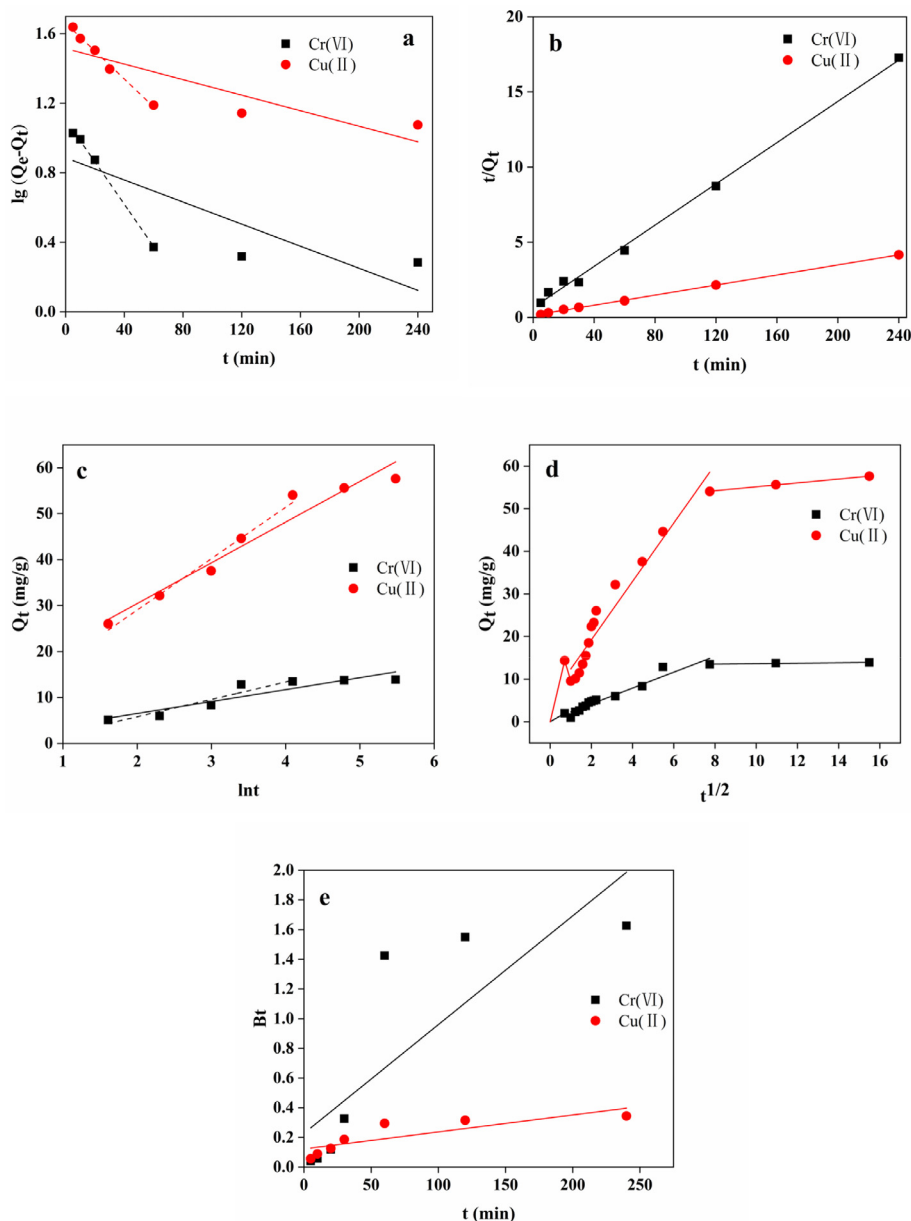

Fig. 10 Linear fitting of the experimental data by geopolymer-cetyltrimethylammonium bromide (GP-CTAB) for the (a) pseudo-first-order, (b) pseudo-second-order, (c) Elovich, (d) Weber-Morris and (e) Boyd equation.

into CTA^+ and transform into CrO_4^{2-} (Li et al., 2017). The adsorption capacity for Cr(VI) is therefore reduced. It can also be seen that under any pH, GP-CTAB has higher adsorption capacity of Cr(VI) than GP where the adsorption capacity of Cu(II) is almost the same. According to the influence of the initial pH on the removal of Cu(II)/Cr(VI), the pH in the following experiments was 5 unless otherwise specified.

3.3. Effect of contact time

The result of contact time is shown in Fig. 7. The adsorption of Cu(II) and Cr(VI) on both geopolymers increases as the contact time increases. GP and GP-CTAB have rapid adsorption in the first 60 min, while for the MK, the adsorption capacity can be negligible. The adsorption capacity of Cr(VI) by GP-CTAB is unchanged at 15.9 mg/g, which is significantly higher than 2.3 mg/g of GP, and the adsorption capacity of Cu(II) is ~69.6 mg/g after 24 h, which is not much different from GP. As shown in Fig. 7c, during the 0–5 min period, the adsorption capacity of Cu(II) and Cr(VI) decreases first and then increases. The reason may be that the initial rate of diffusion of metal ions to the surface of GP-CTAB is too fast and the pore size distribution of GP-CTAB is not uniform. Some of the metal ions cannot be fixed quickly, so they return to the solution.

3.4. Effect of adsorbent dosage

The result of adsorbent dosage is shown in Fig. 8. As the dosage increases, the removal efficiency of Cu(II) by both

geopolymers shows a sharp increasing trend and is almost wholly removed at 1.0 g/L. At the same time, the adsorption capacity shows a downward trend, mainly because of the excess active sites provided by the geopolymer available for adsorption, causing lowering of the adsorption capacity per unit mass. The adsorption of Cr(VI) shows a different trend. First, the removal efficiency of GP-CTAB increases to 25.6% (sorbent dosage is 1.0 g/L), and then decreases to a constant value of ~14.0%.

By comparing the adsorption capacity of GP-CTAB in single/binary system, it is found that the dosage of GP-CTAB in the complete removal of Cu(II) in a binary system (1.0 g/L) is higher than that in a single system (0.6 g/L). The adsorption capacity of Cu(II) is also lower than a single system. In the single and binary systems, the dosage of the maximum removal efficiency of GP-CTAB for Cr(VI) is close to or the same as Cu(II). The GP-CTAB's removal efficiency and adsorption capacity for Cr(VI) in a binary system are higher than a single system. It can be found that the adsorption of Cu(II) by GP-CTAB is suppressed and the adsorption of Cr(VI) is promoted in the Cu(II)/Cr(VI) binary system. The adsorbed geopolymers will undergo ion exchange again in a specific concentration of Na^+ or K^+ solution, and the adsorbed initially ions will desorb (Naghsh and Shams 2017). K^+ ions, which are not present in a single system, exchanges Cu(II) adsorbed by the geopolymers in binary mode. This is equivalent to desorption, and K^+ ions concentration is not too high, so the amount of desorbed Cu(II) is low. Referring to the explanation of similar phenomena (Zhu et al., 2016), as shown in Fig. 9, it is speculated that Cu(II) which is not adsorbed in the solution promotes the

Table 4 Kinetics parameters for Cu(II)/Cr(VI) adsorption onto geopolymer-cetyltrimethylammonium bromide (GP-CTAB) in the binary system.

Kinetics Models	Parameter	Cu(II)	Cr(VI)
Pseudo-first order (0–60 min)	q_e (mg/g)	45.85	12.76
	k_1 ($\times 10^{-4}$ min^{-1})	185.2	280.3
	R^2	0.992	0.997
Pseudo-first order (all contact time)	q_e (mg/g)	32.72	7.690
	k_1 ($\times 10^{-4}$ min^{-1})	73.20	51.40
	R^2	0.664	0.718
Pseudo-second order	q_e (mg/g)	63.55	14.71
	k_2 [g/(mg·min)]	19.07	70.66
	R^2	0.999	0.997
Elovich (0–60 min)	α [mg/(g·min)]	106.7	3.820
	β (g/min)	0.197	0.645
	R^2	0.992	0.996
Elovich (all contact time)	α [mg/(g·min)]	265921.65	4414.22
	β (g/min)	0.426	1.515
	R^2	0.799	0.649
Weber–Morris (0–0.5 min)	k_w [mg/(min$^{1/2}$·g)]	20.29	2.830
	C	0.000	0.000
	R^2	1.000	1.000
Weber–Morris (0.5–1 min)	k_w [mg/(min$^{1/2}$·g)]	−16.39	−3.580
	C	25.94	4.540
	R^2	1.000	1.000
Weber–Morris (1–60 min)	k_w [mg/(min$^{1/2}$·g)]	8.050	2.130
	C	3.070	0.070
	R^2	0.934	0.946
Weber–Morris (60–1440 min)	k_w [mg/(min$^{1/2}$·g)]	0.520	0.090
	C	49.92	12.64
	R^2	0.999	0.972

adsorption of Cr(VI). The adsorption rate of Cr(VI) by GP-CTAB is faster than Cu(II). When Cr(VI) aggregates near the adsorption site, it attracts Cu(II) in solution to maintain electric neutrality and establishes an effective electrostatic shield against the repulsion force between Cr(VI) cations particularly from those in adjacent sites.

This continues to explain the phenomenon that the removal efficiency of Cr(VI) is first increased and then decreased: (1) Since Cu(II) is wholly adsorbed, there is no Cu(II) to promote the adsorption of Cr(VI) in solution. (2) SO_4^{2-} ions exist in a binary system, and SO_4^{2-} has a stronger interference effect on unadsorbed Cr(VI) with the decrease of Cr(VI) concentration. (3) As the dosage continuously increases, although materials are carefully washed, the adsorbent addition increases the solution pH ∼ 0.5–2.0 units during a 24-h equilibration (Luukkonen et al., 2016). This phenomenon was also found in this study. Table 3 shows the results of pH changes before and after adsorption. From Section 3.2, the adsorption of Cr (VI) is very disadvantageous when pH > 6. Based on the above three points, the adsorption capacity of Cr(VI) decreases and affects the removal efficiency, which has a tendency to rise first and then fall. Since GP-CTAB is the best adsorbent, the subsequent studies were performed only using this adsorbent.

3.5. Kinetics

Linear fitting for five kinetic models is presented in Fig. 10. The fitting results are summarised in Table 4. It can be seen that the entire adsorption process for the Cu(II)/Cr(VI) binary system by GP-CTAB follows the pseudo-second-order kinetic equation, and R^2 reaches 0.99 or more, indicating that the whole adsorption process is mainly chemical adsorption (Fayazi, 2019; Ge et al., 2015). As shown in Table 4, the k_2 value of GP-CTAB-adsorbed Cr(VI) is higher than that of Cu(II), indicating that the adsorption rate of Cr(VI) by the geopolymer in the binary system is faster. Also, in the fitting of the pseudo-first-order kinetics in the 0–60 min segment, R^2 reached above 0.99. This shows that the adsorption process of GP-CTAB is accurate using pseudo-first-order kinetics in this period. Combined with the above, it shows that physical adsorption and chemisorption dominate together in the simultaneous adsorption process of GP-CTAB in the range of 0–60 min (Lee et al., 2017; Singhal et al., 2017).

As shown in Table 4 and Fig. 10c, the prophase adsorption of GP-CTAB (within 60 min adsorption time) can be better described by the Elovich kinetic model, in which R^2 reaches 0.99 or higher. However, after the adsorption time exceeds 60 min, the experimental data gradually deviates from the fitted curve. The R^2 over the entire adsorption period is significantly lower than the prophase period, which is consistent with many works of literature (Chen et al., 2018; Barbosa et al., 2018). Therefore, before the equilibrium phase is reached (0–60 min), the adsorption of Cu(II)/Cr(VI) on the surface of GP-CTAB has a non-homogeneous distribution of surface adsorption energy.

The Weber-Morris equation can be used to describe whether the determined step of the mass transfer process was on the surface or internal (Mezenner and Bensmaili, 2009). As shown in Fig. 10d, the adsorption of Cu(II)/Cr(VI) by
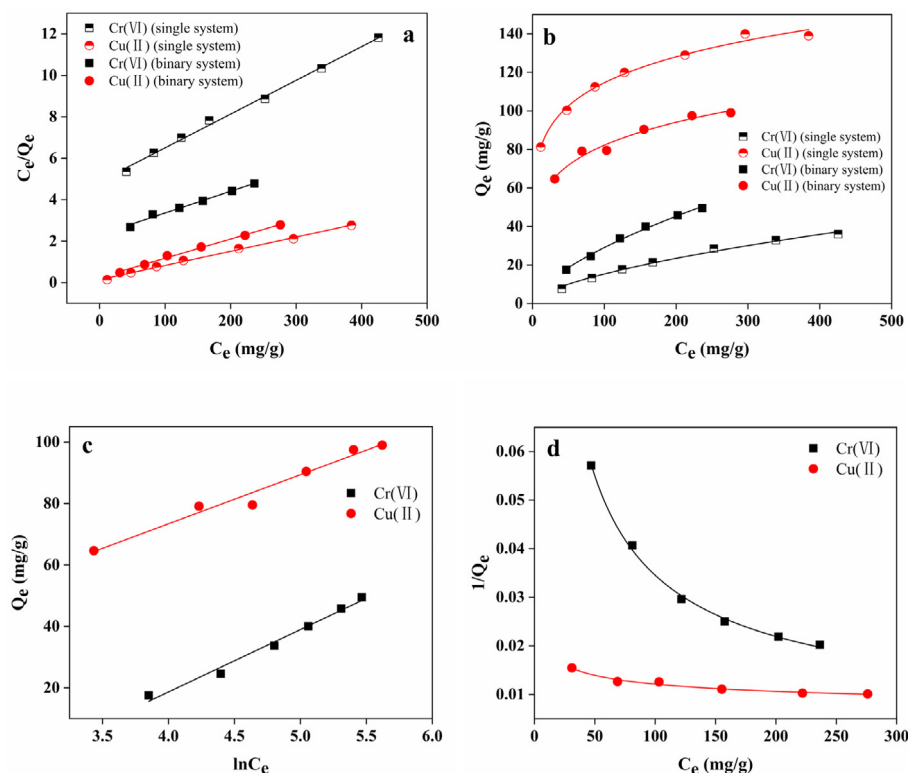

Fig. 11   (a) Langmuir, (b) Freundlich, (c) Temkin, and (d) Sips isotherms for the adsorption of Cu(II)/Cr(VI) onto geopolymer-cetyltrimethylammonium bromide (GP-CTAB).

the GP-CTAB was composed of four stages according to the Weber-Morris model. The fitting results are summarised in Table 4. During the first 0.5 min, Cu(II)/Cr(VI) was rapidly absorbed. However, the slope of the fitting curve in 0.5–1 min was negative, indicating that there was a release process of Cu(II)/Cr(VI) during the first 0.5–1 min. This is consistent with the phenomenon described in Section 3.3. The adsorption was gradually saturated after 60 min. Except for the initial 0–0.5 min portion of the fitting curve, the intercepts of others did not pass through the origin, indicating that a certain boundary layer thickness existed in the adsorption process, and the rate-limiting step is not the intraparticle diffusion but the boundary-layer diffusion (Cheung, et al., 2007; Luukkonen et al., 2016).

To further judge the main steps of the quick control, the Boyd equation is applied for fitting. It can be seen from Fig. 10e that the fitting straight line of Cu(II)/Cr(VI) does not pass through the origin, indicating that the adsorption process is controlled by liquid film diffusion and intraparticle diffusion, and throughout the adsorption process, the outer surface diffused is rate-controlling step (Chen and Wang 2009; Javadian et al., 2015). According to the comprehensive analysis results, in the initial stage of adsorption, the boundary layer diffusion of the outer surface is the adsorption rate control process, and the late adsorption stage is mainly controlled by the intraparticle diffusion.

3.6. Isotherms

In the single system, the initial concentration of Cu(II) and Cr(VI) were adjusted in the range of 50–500 mg/L with pH 5 at 30 °C for 4 h. The tendency for adsorption differs from that of the single system when two ions coexist. Therefore, in the binary system, the concentration of one heavy metal ion was varied from 50 to 300 mg·L^{-1}, while another was fixed at 300 mg·L^{-1}, and other conditions remain unchanged.

Linear fitting for four isotherm models is presented in Fig. 11. The relevant isotherm parameters are summarised in Table 5. The fitting results show that the Langmuir and Freundlich isotherms of GP-CTAB adsorption Cu(II)/Cr(VI) single/binary system can be well fitted. The results show that the adsorption of Cu(II) and Cr(VI) by GP-CTAB is monolayer adsorption, which may be due to the uniform interaction between adsorbed molecules is negligible (Ding et al., 2019). The value of R_L from fitting results in the Langmuir isotherm is between 0 and 1, or the value of n between 1 and 10 in the Freundlich isotherm, indicating that the adsorption process is favourable adsorption (Singhal et al., 2017; Gulnaz et al., 2004). In the binary system, the maximum adsorption capacities of Cu(II) and Cr(VI) fitted by Langmuir were 108.2 mg/g and 95.3 mg/g, respectively. Compared with the single system, the adsorption capacities of Cu(II) is decreased, and Cr(VI) is increased, which is consistent with the inhibition and promotion phenomenon found in this study. The Temkin isotherm is well-

Table 5 Isotherm parameters for Cu(II)/Cr(VI) adsorption onto geopolymer-cetyltrimethylammonium bromide (GP-CTAB).

Isotherm Models	Parameter	Cu(II)	Cr(VI)
Langmuir (single system)	Q_e (mg/g)	147.1	61.30
	b (mg^{-1})	0.048	0.004
	R_L	0.040	0.330
	R^2	0.997	0.996
Langmuir (binary system)	Q_e (mg/g)	108.2	95.30
	b (mg^{-1})	0.037	0.005
	R_L	0.080	0.400
	R^2	0.996	0.989
Freundlich (single system)	K_f	54.69	0.68
	n	6.230	1.500
	R^2	0.993	0.992
Freundlich (binary system)	K_f	33.26	1.390
	n	5.090	1.520
	R^2	0.980	0.997
Temkin (binary system)	A_T (L/mol)	1.810	0.050
	b_T (J/mol)	157.8	124.2
	R^2	0.973	0.986
Sips (binary system)	Q_{ms} (mg/g)	274.7	555.6
	γ	0.280	0.700
	K_S	0.0005	0.0002
	R^2	0.980	0.997

Table 6 Adsorption results of Cu(II) and Cr(VI) onto different adsorbents from literature reports.

Sorbent	Q_{max} (mg/g)		Sorbent dose (g/L)	Time (°C)	Adsorption time (h)	Ref.
	Cu (II)	Cr (VI)				
β-cyclodextrin polymers	164.4	–	0.5	45	24	He et al. (2017)
Metakaolin based geopolymers	44.73	–	10.0	–	7	Andrejkovičová et al. (2016)
Fly ash and iron ore tailing based geopolymers	113.4	–	3.0	20	1.5	Duan et al. (2016)
CTAB modified geopolymers	40.00	–	0.4	–	2	Singhal et al. (2017)
Wheat straw amphoteric adsorbent	73.53	227.3	2	20	6	Zhong et al. (2013)
Tannin-immobilized nanocellulose	51.85	94.90	0.5	–	12	Xu et al. (2017)
Nitrogen-doped chitosan-Fe(III) composite(Binary system)	165.8	405.5	13.72	30	36	Zhu et al. (2016)
Surfactant–modified serpentine	–	55.86	2	30	2	Mobarak et al. (2019)
Hierarchical porous Ni/Co-LDH hollow dodecahedron	–	99.90	0.4	30	12	Hu et al. (2019)
Mesoporous carbon nitride	–	48.31	1	25	48	Chen et al. (2014)
CTAB modified geopolymers(Single system)	147.1	61.30	0.4	30	4	Present study
CTAB modified geopolymers(Binary system)	108.2	95.30	0.4	30	4	Present study

fitted; the adsorption process has both physical adsorption and chemical adsorption (Araújo et al., 2018; Wang et al., 2012). Even if the Sips isotherm was well-fitted, the amount of adsorption is different from the actual situation. Similar phenomena are found in the literature (Barbosa et al., 2018). The determination coefficients of four models are all higher than 0.970, which indicates that the adsorption process is similar to monolayer chemical adsorption and has certain surface non-uniformities. The mechanism of the adsorption process is complex (Buasri et al., 2007). It is further confirmed that the adsorption of GP-CTAB is mainly chemical and ion exchange adsorption between the adsorbate molecules and the adsorbent.

In Table 6, the maximum adsorption capacity fit by Langmuir was selected to compare the adsorption capacities of Cu(II) and Cr(VI) with different adsorbents reported in the literature. It can be seen that the geopolymer obtained in this study has a higher adsorption capacity for Cu(II) and Cr(VI), and has the advantage of being simultaneously adsorbable. Also, GP-CTAB can be prepared from low-cost waste. Therefore, GP-CTAB can be considered as a new type of low-cost adsorbent.

4. Conclusion

A novel mesoporous geopolymer was synthesised by using metakaolin as silicon and alumina raw materials and CTAB as an organic modifier. Compared with conventional geopolymers, GP-CTAB's properties for adsorbing metal cations is only slightly reduced, but can significantly adsorb anionic forms of metals, and conventional geopolymers do not have this ability. After organic modification, the prepared product still belongs to the geopolymer classification, which differs from the traditional geopolymer in that the surface is attached to a quaternary ammonium salt cation. In the Cu(II)/Cr(VI) binary system, the adsorption of Cu(II) is slightly reduced by the influence of interfering ions, and Cr(VI) may be promoted by electrostatic shielding caused by unadsorbed Cu(II) in the solution. No Cu(II) ions in the solution improve the presence of interfering ions, and the increase of pH during adsorption are the reasons for the removal rate of Cr(VI) ions rise first and then decreases. The maximum adsorption capacities of Cu(II) and Cr(VI) in binary systems were 108.2 mg/g and 95.3 mg/g, respectively. GP-CTAB can be in competition with other similar adsorbents, with a specific utilisation prospect.

Data availability

The raw/processed data required to reproduce these findings cannot be shared at this time as the data also forms part of an ongoing study.

References

Andrejkovičová, S., Sudagar, A., Rocha, J., Patinha, C., Hajjaji, W., da Silva, E.F., Velosa, A., Rocha, F., 2016. The effect of natural zeolite on microstructure, mechanical and heavy metals adsorption properties of metakaolin based geopolymers. Appl. Clay Sci. 126, 141–152.

Araújo, C.S.T., Almeida, I.L.S., Rezende, H.C., Marcionilio, S.M.L.O., Léon, J.J.L., de Matos, T.N., 2018. Elucidation of mechanism involved in adsorption of Pb(II) onto lobeira fruit (Solanum lycocarpum) using Langmuir, Freundlich and Temkin isotherms. Microchem. J. 137, 348–354.

Aslan, D.I., Özoğul, B., Ceylan, S., Geyikçi, F., 2018. Thermokinetic analysis and product characterization of Medium Density Fiberboard pyrolysis. Bioresour. Technol. 258, 105–110.

Barbosa, T.R., Foletto, E.L., Dotto, G.L., Jahn, S.L., 2018. Preparation of mesoporous geopolymer using metakaolin and rice husk ash as synthesis precursors and its use as potential adsorbent to remove organic dye from aqueous solutions. Ceram. Int. 44, 416–423.

Buasri, A., Yongbut, P., Phattarasirichot, K., 2007. Adsorption equilibrium of zinc ions from aqueous solution by using modified clinoptilolite. Chiang Mai J. Sci. 35, 56–62.

Cai, W., Gu, M., Jin, W., Zhou, J., 2019. CTAB-functionalized C@SiO2 double-shelled hollow microspheres with enhanced and selective adsorption performance for Cr(VI). J. Alloys Compd. 777, 1304–1312.

Chen, H., Wang, A., 2009. Adsorption characteristics of Cu(II) from aqueous solution onto poly(acrylamide)/attapulgite composite. J. Hazard. Mater. 165, 223–231.

Chen, H., Yan, T., Jiang, F., 2014. Adsorption of Cr(VI) from aqueous solution on mesoporous carbon nitride. J. Taiwan Inst. Chem. Eng. 45, 1842–1849.

Chen, Y., Wang, B., Xin, J., Sun, P., Wu, D., 2018. Adsorption behavior and mechanism of Cr(VI) by modified biochar derived from Enteromorpha prolifera. Ecotoxicol. Environ. Saf. 164, 440–447.

Cheung, W.H., Szeto, Y.S., McKay, G., 2007. Intraparticle diffusion processes during acid dye adsorption onto chitosan. Bioresour. Technol. 98, 2897–2904.

Davidovits, J., Davidovits, M., Davidovits, N., 1994. Process for obtaining a geopolymeric alumino-silicate and products thus obtained, US.

Ding, P., Song, W., Wang, C., Yu, Z., 2019. Adsorption of Cu(II) and Pb(II) from aqueous solutions onto a metakaolin-based geopolymer. Desalin. Water Treat. 158, 164–173.

Duan, P., Yan, C., Zhou, W., Ren, D., 2016. Development of fly ash and iron ore tailing based porous geopolymer for removal of Cu(II) from wastewater. Ceram. Int. 42, 13507–13518.

Fayazi, M., 2019. Facile hydrothermal synthesis of magnetic sepiolite clay for removal of Pb(II) from aqueous solutions. Anal. Bioanal. Chem. Res. 147, 87–96.

Ge, Y., Cui, X., Kong, Y., Li, Z., He, Y., Zhou, Q., 2015. Porous geopolymeric spheres for removal of Cu(II) from aqueous solution: synthesis and evaluation. J. Hazard. Mater. 283, 244–251.

Gulnaz, O., Kaya, A., Matyar, F., Arikan, B., 2004. Sorption of basic dyes from aqueous solution by activated sludge. J. Hazard. Mater. 108, 183–188.

He, J., Li, Y., Wang, C., Zhang, K., Lin, D., Kong, L., Liu, J., 2017. Rapid adsorption of Pb, Cu and Cd from aqueous solutions by β-cyclodextrin polymers. Appl. Surf. Sci. 426, 29–39.

Hu, H., Liu, J., Xu, Z., Zhang, L., Cheng, B., Ho, W., 2019. Hierarchical porous Ni/Co-LDH hollow dodecahedron with excellent adsorption property for Congo red and Cr(VI) ions. Appl. Surf. Sci. 478, 981–990.

Javadian, H., Ghorbani, F., Tayebi, H.-A., Asl, S.H., 2015. Study of the adsorption of Cd (II) from aqueous solution using zeolite-based geopolymer, synthesized from coal fly ash; kinetic, isotherm and thermodynamic studies. Arabian J. Chem. 8, 837–849.

Kara, İ., Yilmazer, D., Akar, S.T., 2017. Metakaolin based geopolymer as an effective adsorbent for adsorption of zinc(II) and nickel (II) ions from aqueous solutions. Appl. Clay Sci. 139, 54–63.

Król, M., Minkiewicz, J., Mozgawa, W., 2016. IR spectroscopy studies of zeolites in geopolymeric materials derived from kaolinite. J. Mol. Struct. 1126, 200–206.

Landaburu-Aguirre, J., Pongrácz, E., Perämäki, P., Keiski, R.L., 2010. Micellar-enhanced ultrafiltration for the removal of cadmium and zinc: use of response surface methodology to improve understanding of process performance and optimisation. J. Hazard. Mater. 180, 524–534.

Lee, N.K., Khalid, H.R., Lee, H.K., 2017. Adsorption characteristics of cesium onto mesoporous geopolymers containing nano-crystalline zeolites. Microporous Mesoporous Mater. 242, 238–244.

Lee, S.Y., Kim, S.J., 2002. Adsorption of naphthalene by HDTMA modified kaolinite and halloysite. Appl. Clay Sci. 22, 55–63.

Li, L., Wang, S., Zhu, Z., 2006. Geopolymeric adsorbents from fly ash for dye removal from aqueous solution. J. Colloid Interface Sci. 300, 52–59.

Li, N., Fu, F., Lu, J., Ding, Z., Tang, B., Pang, J., 2017. Facile preparation of magnetic mesoporous MnFe2O4@SiO2-CTAB composites for Cr(VI) adsorption and reduction. Environ. Pollut. 220, 1376–1385.

Li, Z., Beachner, R., McManama, Z., Hanlie, H., 2007. Sorption of arsenic by surfactant-modified zeolite and kaolinite. Microporous Mesoporous Mater. 105, 291–297.

Liang, Z., Zhaob, Z., Sun, T., Shi, W., Cui, F., 2016. Adsorption of quinolone antibiotics in spherical mesoporous silica: effects of the retained template and its alkyl chain length. J. Hazard. Mater. 305, 8–14.

Liu, Y., Yan, C., Zhang, Z., Wang, H., Zhou, S., Zhou, W., 2016. A comparative study on fly ash, geopolymer and faujasite block for Pb removal from aqueous solution. Fuel 185, 181–189.

Louati, S., Baklouti, S., Samet, B., 2016. Acid based geopolymerization kinetics: Effect of clay particle size. Appl. Clay Sci. 132–133, 571–578.

Luukkonen, T., Runtti, H., Niskanen, M., Tolonen, E.T., Sarkkinen, M., Kemppainen, K., Ramo, J., Lassi, U., 2016. Simultaneous removal of Ni(II), As(III), and Sb(III) from spiked mine effluent with metakaolin and blast-furnace-slag geopolymers. J. Environ. Manage. 166, 579–588.

Majeed, J., Ramkumar, J., Chandramouleeswaran, S., Jayakumar, O. D., Tyagi, A.K., 2013. Kinetic modeling: dependence of structural and sorption properties of ZnO – Crucial role of synthesis. RSC Adv. 3, 3365.

Maleki, A., Hajizadeh, Z., Sharifi, V., Emdadi, Z., 2019. A green, porous and eco-friendly magnetic geopolymer adsorbent for heavy metals removal from aqueous solutions. J. Cleaner Prod. 215, 1233–1245.

Messina, F., Ferone, C., Molino, A., Roviello, G., Colangelo, F., Molino, B., Cioffi, R., 2017. Synergistic recycling of calcined clayey sediments and water potabilization sludge as geopolymer precursors: upscaling from binders to precast paving cement-free bricks. Constr. Build. Mater. 133, 14–26.

Mezenner, N.Y., Bensmaili, A., 2009. Kinetics and thermodynamic study of phosphate adsorption on iron hydroxide-eggshell waste. Chem. Eng. J. 147, 87–96.

Mihaly-Cozmuta, L., Mihaly-Cozmuta, A., Peter, A., Nicula, C., Tutu, H., Silipas, D., Indrea, E., 2014. Adsorption of heavy metal cations by Na-clinoptilolite: equilibrium and selectivity studies. J. Environ. Manage. 137, 69–80.

Mobarak, M., Mohamed, E.A., Selim, A.Q., Sellaoui, L., Lamine, A. B., Erto, A., Bonilla-Petriciolet, A., Seliem, M.K., 2019. Surfactant–modified serpentine for fluoride and Cr(VI) adsorption in single and binary systems: experimental studies and theoretical modeling. Chem. Eng. J. 369, 333–343.

Morsy, M.S., Alsayed, S.H., Al-Salloum, Y., Almusallam, T., 2014. Effect of sodium silicate to sodium hydroxide ratios on strength and microstructure of fly ash geopolymer binder. Arab. J. Sci. Eng. 39, 4333–4339.

Naghsh, M., Shams, K., 2017. Synthesis of a kaolin-based geopolymer using a novel fusion method and its application in effective water softening. Appl. Clay Sci. 146, 238–245.

Provis, L.J., 2014. Geopolymers and other alkali activated materials: why, how, and what?. Mater. Struct. 47, 11–25.

Qiu, R., Cheng, F., Huang, H., 2018. Removal of Cd2+ from aqueous solution using hydrothermally modified circulating fluidized bed fly ash resulting from coal gangue power plant. J. Cleaner Prod. 172, 1918–1927.

Sarkar, C., Basu, J.K., Samanta, A.N., 2017. Removal of Ni 2+ ion from waste water by Geopolymeric Adsorbent derived from LD Slag. J. Water Process Eng. 17, 237–244.

Singhal, A., Gangwar, B.P., Gayathry, J.M., 2017. CTAB modified large surface area nanoporous geopolymer with high adsorption capacity for copper ion removal. Appl. Clay Sci. 150, 106–114.

Siyal, A.A., Shamsuddin, M.R., Khan, M.I., Rabat, N.E., Zulfiqar, M., Man, Z., Siame, J., Azizli, K.A., 2018. A review on geopolymers as emerging materials for the adsorption of heavy metals and dyes. J. Environ. Manage. 224, 327–339.

Song, Y., Liu, J., Evrendilek, F., Kuo, J., Buyukada, M., 2019. Combustion behaviors of Pteris vittata using thermogravimetric, kinetic, emission and optimization analyses. J. Cleaner Prod., 237

Tang, Q., Wang, K., Yaseen, M., Tong, Z., Cui, X., 2018. Synthesis of highly efficient porous inorganic polymer microspheres for the adsorptive removal of Pb 2+ from wastewater. J. Cleaner Prod. 193, 351–362.

Wan Ngah, W.S., Hanafiah, M.A.K.M., 2008. Removal of heavy metal ions from wastewater by chemically modified plant wastes as adsorbents: a review. Bioresour. Technol. 99, 3935–3948.

Wang, W.Q., Ming-Yu, L.I., Zeng, Q.X., 2012. Thermodynamics of Cr (VI) adsorption on strong alkaline anion exchange fiber. Trans. Nonferrous Metals Soc. China 22, 2831–2839.

Xu, F., Wang, B., Yang, D., Hao, J., Qiao, Y., Tian, Y., 2018. Thermal degradation of typical plastics under high heating rate conditions by TG-FTIR: pyrolysis behaviors and kinetic analysis. Energy Convers. Manage. 171, 1106–1115.

Xu, Q., Wang, Y., Jin, L., Wang, Y., Qin, M., 2017. Adsorption of Cu (II), Pb (II) and Cr (VI) from aqueous solutions using black wattle tannin-immobilized nanocellulose. J. Hazard. Mater. 339, 91–99.

Xu, Y., Chen, J., Chen, R., Yu, P., Guo, S., Wang, X., 2019. Adsorption and reduction of chromium(VI) from aqueous solution using polypyrrole/calcium rectorite composite adsorbent. Water Res. 160, 148–157.

Yunsheng, Z., Wei, S., Qianli, C., Lin, C., 2007. Synthesis and heavy metal immobilization behaviors of slag based geopolymer. J. Hazard. Mater. 143, 206–213.

Zhong, Q.-Q., Yue, Q.-Y., Gao, B.-Y., Li, Q., Xu, X., 2013. A novel amphoteric adsorbent derived from biomass materials: synthesis and adsorption for Cu(II)/Cr(VI) in single and binary systems. Chem. Eng. J. 229, 90–98.

Zhu, C., Liu, F., Zhang, Y., Wei, M., Zhang, X., Ling, C., Li, A., 2016. Nitrogen-doped chitosan-Fe(III) composite as a dual-functional material for synergistically enhanced co-removal of Cu(II) and Cr (VI) based on adsorption and redox. Chem. Eng. J. 306, 579–587.